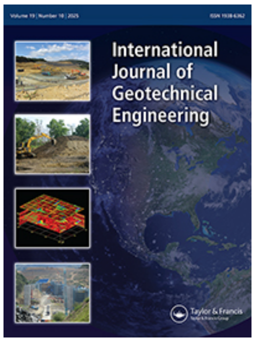

Taylor & Francis
Taylor & Francis Group

International Journal of Geotechnical Engineering

ISSN: 1938-6362 (Print) 1939-7879 (Online) Journal homepage: www.tandfonline.com/journals/yjge20

Wing ratio effect on the failure mechanism and uplift behaviour of helical anchors in sand

Hamed Nuri, Hossein Salehzadeh, Ali Akbar Heshmati Rafsanjani, Cristina de Hollanda Cavalcanti Tsuha & Amin Askarinejad

To cite this article: Hamed Nuri, Hossein Salehzadeh, Ali Akbar Heshmati Rafsanjani, Cristina de Hollanda Cavalcanti Tsuha & Amin Askarinejad (2025) Wing ratio effect on the failure mechanism and uplift behaviour of helical anchors in sand, International Journal of Geotechnical Engineering, 19:10, 923-942, DOI: 10.1080/19386362.2025.2574591

To link to this article: https://doi.org/10.1080/19386362.2025.2574591

Published online: 21 Oct 2025.

INTERNATIONAL JOURNAL OF GEOTECHNICAL ENGINEERING
2025, VOL. 19, NO. 10, 923–942
https://doi.org/10.1080/19386362.2025.2574591

Taylor & Francis
Taylor & Francis Group

Wing ratio effect on the failure mechanism and uplift behaviour of helical anchors in sand

Hamed Nuri [a], Hossein Salehzadeh [a], Ali Akbar Heshmati Rafsanjani [a], Cristina de Hollanda Cavalcanti Tsuha [b] and Amin Askarinejad [c]

[a]School of Civil Engineering, Iran University of Science and Technology, Narmak, Iran; [b]Department of Geotechnical Engineering, University of São Paulo at São Carlos São Carlos, Brazil; [c]Faculty of Civil Engineering and Geosciences, Delft University of Technology Delft, The Netherlands

ABSTRACT

Helical anchors are load-resisting elements, installed vertically or inclined to resist uplift or combined loads. The geometry of these anchors significantly impacts their uplift resistance. Wing Ratio (i.e. helix diameter/shaft diameter) is a notable aspect of anchor geometry because of its influence on installation requirements and uplift capacity. This study is aimed at exploring the impact of WR on anchor uplift capacity and failure mechanisms. Through a series of centrifuge tests on small-scale half-models of helical anchors, it was observed that increasing WR led to corresponding increase in uplift capacity. However, this was accompanied by decrease in both peak helix pressure (peak uplift capacity/helix area) and the breakout factor Nqu, indicating reduced load-bearing efficiency. This decline is attributed to increased soil disturbance resulting from larger WRs. Additionally, while WR did not influence the formation of failure mechanisms, it exhibited some influence on determining the critical embedment depth in medium-dense sand.

ARTICLE HISTORY
Received 19 May 2025
Accepted 22 September 2025

KEYWORDS
Helical anchors; Centrifuge modelling; Wing ratio; Failure mechanism; Uplift capacity

Introduction

Screw anchors are load-bearing components comprising a central shaft with one or more helices welded to it. These anchors have numerous onshore applications, including foundations for guyed tower cables and transmission power lines. A new application for these anchors in the offshore environment was introduced by (Spagnoli et al. 2015) and studied in detail by many researchers such as (M. J. Brown et al. 2019; Cerfontaine et al. 2020; Davidson et al. 2019, 2022) and (Spagnoli and de Hollanda Cavalcanti Tsuha 2020).

Although several studies have examined the axial and lateral capacity of screw anchors and their installation demands, relatively few have explored the specific failure mechanisms of these structures under axial or lateral loading in sandy soils. Moreover, industry practices and prior experience highlight that configuration of helices plays a pivotal role in both installation requirements and the peak uplift capacity of anchors. Among these geometric factors, the wing ratio (WR) stands out as a critical parameter that has not yet been thoroughly researched. The WR has been shown to affect the vertical installation force (crowd), torque, and peak uplift capacity of helical anchors (Spagnoli et al. 2015).

Further research is therefore necessary to deepen our understanding of how the WR influences installation demands, peak uplift capacity, and governing failure mechanisms. Such comprehensive insights are vital for improving the predictive accuracy of uplift capacity models for helical anchors and ensuring their suitability for large-scale industrial applications.

Wing ratio

To date, only a limited number of studies have evaluated the effect of the wing ratio (WR) on the uplift capacity of helical anchors. WR, defined as the ratio of the helical plate diameter to the shaft diameter, $\left(WR = \frac{D}{d}\right)$, is a crucial design parameter for offshore screw anchors. This enables engineers to design screw anchor geometries that provide the required uplift capacity while minimizing the installation torque (M. Brown 2019).

One of the earliest studies to examine the influence of WR on the failure mechanisms of helical anchors was conducted by (Nagata and Hirata 2005) where they examined the effects of WR, helix embedment and diameter on the uplift capacity and failure surface of helical anchors in dense sand (84% relative density). The tests were conducted on reduced-scale models under 1g

CONTACT Hamed Nuri nuri_hamed@civileng.iust.ac.ir School of Civil Engineering, Iran University of Science and Technology, Narmak, University St., Hengam St., Resalat Square, Tehran 1684613114, Iran

gravity conditions with (H/D) = 1 ~ 13. The study found that increasing the WR led to higher uplift capacity but resulted in a decrease in uplift pressure on the helices. Additionally, the observed failure surface was reported as a reversed truncated cone, with a reduced inclination (with vertical) at the upper portion of the failure cone.

(Urabe et al. 2015) investigated the impact of WR on the cyclic and monotonic axial responses of wing piles using centrifuge modelling, focusing on four distinct WRs in very dense Toyoura sand. The wing piles consisted of a shaft and a flat plate attached to it near the tip and were installed in the soil as wished-in-place. Their findings indicated that WR has a substantial influence on the cyclic pullout capacity of the piles, whereas the cyclic compression response is largely governed by shaft resistance. The failure surface, however, was not visualized in these tests.

(Spagnoli et al. 2015) conducted experiments on 1/10 scale single-helix screw piles with varying WRs to assess the effects of WR on installation torque and uplift capacity. The experiments were carried out in a 1 × 1 × 1 m tank under 1 g conditions, with piles installed using an electric drill to the intended depth. Results showed that WR values of 1.5 and 2 yielded the lowest installation torque-to-capacity ratios, suggesting these WRs offer optimized installation efforts with regards to uplift capacity.

In an experimental study (Nazir et al. 2014), conducted monotonic uplift tests on small-scale helical anchor models to investigate the influence of the shaft-to-helix diameter ratio ($\frac{1}{WR}$) on the uplift capacity and failure mechanisms of single-helix piles. The helical plate diameter was kept constant, while the shaft diameter was varied to achieve different shaft-to-helix diameter ratios. The piles were installed as wished-in-place in a sand container and tested under 1 g conditions. The results indicated a wide range of N_{qu} values (N_{qu} = 2 ~ 92) for the H/D ranges examined (1 ~ 5) in both loose and dense sand conditions. The shaft-to-helix diameter ratio exhibited negligible influence on N_{qu} which was attributed to the limited contribution of shaft skin friction to uplift resistance Alternatively, this outcome may also be explained by the absence of installation effects, which can loosen the soil above the helix and influence uplift capacity.

More recently, da Silva and Tsuha (2021) conducted tests on the helix portion of helical anchors to examine the influence of WR and confining pressure on installation forces and load-bearing performance. In these tests, anchors were installed under pitch-matched conditions in a calibration chamber. Pitch-matched installation (also referred to as perfect installation) is defined as a mode in which the anchor advances one pitch per revolution into the foundation soil. The study reported that increasing WR reduced the peak uplift pressure, while peak compressive pressure remained unchanged. In this context, uplift/compressive pressure was defined as the peak uplift/compressive load divided by the helix bearing area. The authors also observed the formation of a cylindrical failure surface above the helix.

Given the scarcity of research on the effects of WR on the uplift capacity of helical anchors and the inconsistency between different studies e.g. between the results of Tsuha et al. (2019) and Nazir et al. (2014), establishing a clear correlation between WR and anchor uplift capacity is essential for improving helical anchor design.

Failure mechanism

Previous research efforts have explored the general failure mechanisms of helical anchors through physical modelling. More recent studies, such as those by (Nazir et al. 2014) and (Hao et al. 2019) have focused on specific conditions to isolate installation effects and evaluate the influence of other key parameters. Gaining insight into governing failure mechanisms and their influencing factors (such as WR) is expected to improve the accuracy of anchor design methods and clarify how individual helices interact with each other and with nearby anchors. Therefore, investigating the failure mechanisms of helical anchors across different geometrical configurations and geotechnical conditions is essential for advancing both their design and practical use.

In single-helix anchors, two primary failure modes are commonly observed: shallow and deep (Perko 2009). The shallow failure mode is characterized by a failure surface resembling a truncated inverted cone and is typically accompanied by soil swelling near the ground surface. In contrast, the deep failure mode involves a failure surface that does not reach the ground surface, remaining localized around the anchor, accompanied by the development of a flow-around mechanism.

Several studies have investigated the failure mechanisms of helical piles and anchors under various conditions, utilizing both experimental and numerical approaches. Ghaly, Hanna, and Hanna (1991) conducted experiments on medium-scale helical anchor models in a test tank with different sand densities. They observed a truncated cone failure surface inclined at approximately 2φ/3 to the vertical within the tested range (H/B = 2 ~ 16).

Liu, Liu, and Zhu (2012) performed small-scale tests on model plate anchors embedded in poorly graded loose and dense sand, observed through a Perspex window, under 1 g conditions without any surcharge. The authors noted that the failure plane exhibited a conical shape for all tested anchors (H/D = 1 ~ 9), inclined at φ/4 to the vertical.

Giampa, Bradshaw, and Schneider (2017) conducted an experimental study on medium-scale helical anchors (helix diameter D = 152 and 254 mm) installed in dense sand, comparing the findings with results from finite element analyses. They concluded that the failure surface was a truncated cone with an inclination of ψ (with ψ representing dilation angle of the sand at the corresponding confining stress and relative density) for the tested H/D range (H/D = 1.8 ~ 7.1).

Nagai, Tsuchiya, and Shimada (2018) reported the results of tests on small-scale helical anchors installed in loose and dense sand under 1 g conditions. They explored the impact of installation methods on helical anchor performance and failure surfaces, using anchors with a WR of 2 within a 1 × 1 × 1 m calibration chamber. Anchors were embedded to a depth of 5D using forward, reverse, and boring installation techniques. The findings revealed that forward installation produced a cylindrical failure surface, whereas boring installation resulted in a bowl-shaped profile.

(Chen et al. 2020) conducted experimental and DEM studies on the compressive bearing capacity of a partially screwed shaft in medium-dense sand, observed through a Perspex window without considering installation disturbances. It was concluded that the screw sections made a significant contribution to the shaft's compressive capacity, and a bubble-shaped failure surface surrounding these sections was reported. Cerfontaine et al. (2023) carried out a numerical study on helical anchors using the discrete element method (DEM) to investigate the effect of the installation advancement rate (AR) on the resulting failure mechanisms. The study revealed that the failure surface exhibited a wedge shape in the shallow failure mode, while a flow-around mechanism developed in the deep mode (H/D = 7.6 ~ 8.5).

Understanding the failure mechanisms and parameters influencing them is essential, especially considering the significant soil disturbance induced during anchor installation and the necessity of a robust analytical framework for predicting anchor uplift capacity (Schiavon, de Hollanda Cavalcanti Tsuha, and Thorel 2016). Therefore, in light of the knowledge gap concerning the failure mechanisms of helical anchors with varying geometries, particularly those with different WRs, this study aims to examine this aspect in greater depth.

In the present research, anchor-induced soil disturbance during installation was simulated using a simple and reproducible technique. This approach, as employed by (Salehzadeh, Nuri, and Rafsanjani 2022), is intended to provide a deeper understanding of the failure mechanisms of helical anchors with varying geometries.

Accordingly, six centrifuge tests were conducted to investigate the failure mechanism, the mobilized soil mass during pullout, and peak uplift capacity of helical anchors in medium-dense sand, with an emphasis on WR effects under monotonic loading conditions. Additionally, the uplifting performance was further analysed by comparing helix pressure and dimensionless breakout factor (N_{qu}) with findings from two pertinent previous studies. The geometry of the resulting gaps was also examined, potentially valuable for future investigations into the cyclic loading behaviour of helical anchors.

Materials and methods

Model soil

#161 Firoozkooh sand was used in the current study as a standard test soil, employed in numerous previous studies such as Baziar, Shahnazari, and Kazemi 2018; Heshmati Rafsanjani, Salehzadeh, and Nuri (2021) and Sabermahani and Nuri (2021). The tested sand has a mean grain size diameter of 0.25 mm and is classified as SP according to the USCS. The mechanical and physical properties together with the grain size distribution of this soil are presented in Figure 1 and Table 1, respectively.

The sand was prepared using the pluviation technique in a medium-dense state ($D_r = 60\%$) inside a rectangular box with dimensions of 500 × 280 × 240 mm (L×W×H). Sand density was measured in each test using two small calibration cylinders placed at the bottom of the strongbox. The peak internal friction angle (φ_{peak}) of the sand was determined according to the results of triaxial tests performed by previous researchers such as Hasanlourad, Khatami, and Ahmadi (2018). The median sand density and confining pressure (at the level of the helix) were 60% and 30 ~ 50 kPa, respectively.

Loading and data acquisition system

The loading and data acquisition system elaborated in Heshmati Rafsanjani, Salehzadeh, and Nuri (2021) was used to apply the loads and record the output data. The loading system comprised a screw jack connected to the stepper motor via a pulley that transferred the load to the test anchor head through a hook. Forces were also measured using a SEWHA-CNM SM603 loadcell. Figure 2 shows a schematic diagram of the test setup.

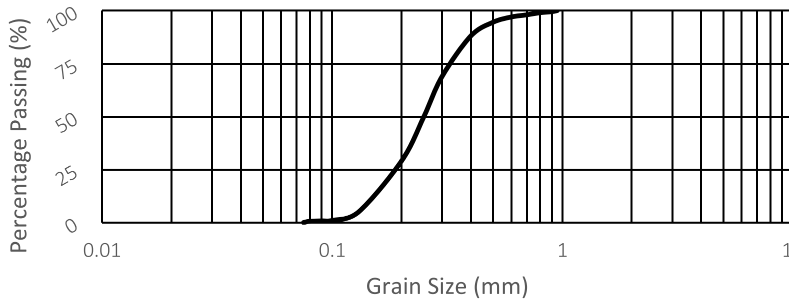

Figure 1. The grain size distribution of the #161 firoozkooh sand.

Table 1. Mechanical and physical properties of #161 Firoozkooh sand ($D_r = 60\%$).

USCS grade	C_c	C_u	d_{50} (mm)	e_{min}	e_{max}	G_s	c (kPa)	φ_{cs} (°)	φ_{peak}(°)
SP	0.88	1.87	0.25	0.55	0.87	2.658	0	29	35

Particle image velocimetry (PIV)

The Particle Image Velocimetry (PIV) technique, originally introduced for fluid flow experiments, was adapted for geotechnical testing (White, Take, and Bolton 2003) and further developed by (Stanier and White 2013) and others. PIV analysis offers a rapid and precise method for measuring displacements of objects within the field of view (FOV). In the present study, model video footage during testing was recorded using a SONY DSC-TX30 camera, and relevant frames were extracted and processed with the GeoPIV-RG code in MATLAB. A row of LED lights ensured adequate illumination of the Perspex window.

Helical anchor model

The anchor models were fabricated from aluminium to match the roughness properties of those used in (Heshmati Rafsanjani, Salehzadeh, and Nuri 2021). The shaft diameter was kept constant across all anchors, while the helix diameter was varied to achieve different WRs. To obtain realistic results, the pitch of the helix was simulated using an inclined half-helix. Friction at the Perspex–anchor interface was minimized by applying silicone oil, as described by Stanier, Black, and Hird (2014) and Chen et al. (2018). Detailed specifications of the models are provided in Table 2.

The present study specifically focuses on the geotechnical aspects of soil–structure interaction, without accounting for the potential structural buckling or failure of the anchor system. Post-test inspections of the anchors following each pullout test confirmed this assumption, revealing no visible signs of buckling or failure in either the plate or the plate-shaft connection.

Particle size effects on the uplift capacity were also minimized by considering $W/d_{50} > 16$ according to (Heshmati Rafsanjani, Salehzadeh, and Nuri 2021) who reported no scale effects on the net uplift capacity of helical anchors for $W/d_{50} > 16$. Furthermore, the D/d_{50} ratio in the present study varied between 64 and 96, exceeding the recommendations of (Garnier et al. 2007) for plate anchors, which suggest $D/d_{50} > 48$ to minimize scale effects.

Installation procedure and verification of the testing method

Accurately reproducing installation disturbances remains a significant challenge in the modelling of helical anchors. In this study, the installation disturbance was not fully replicated (e.g. stress redistribution due to installation was not reproduced) due to several limitations, including the absence of a stress regeneration system, such as those used in calibration chamber tests and uncertainties regarding critical parameters, such as the precise stress distribution around the anchor post-installation and its dependence on anchor geometry.

While certain limitations may have had a minor influence on the observed failure mechanisms, the PIV results still provide valuable insights. Moreover, the findings of this study align with trends reported in previous model studies conducted under field-like stress conditions such as Nagata and Hirata (2005) and da Silva and Tsuha (2021). Study (Nagata and Hirata 2005) demonstrated that N_{qu} decreases with increasing WR at a given relative embedment depth Figure 9b). In da Silva and Tsuha (2021), although N_{qu} values were not compared at the same H/D ratio, Figure 9a shows that a WR of 2 under 50 kPa yielded a higher N_{qu} than a WR of 4 under 100 kPa. A similar trend is observed in the present study (Figure 8), further supported by the PIV analysis.

The alteration in sand density, a primary consequence of the installation process in the surrounding soil, was modelled by pluviating the sand at a relative

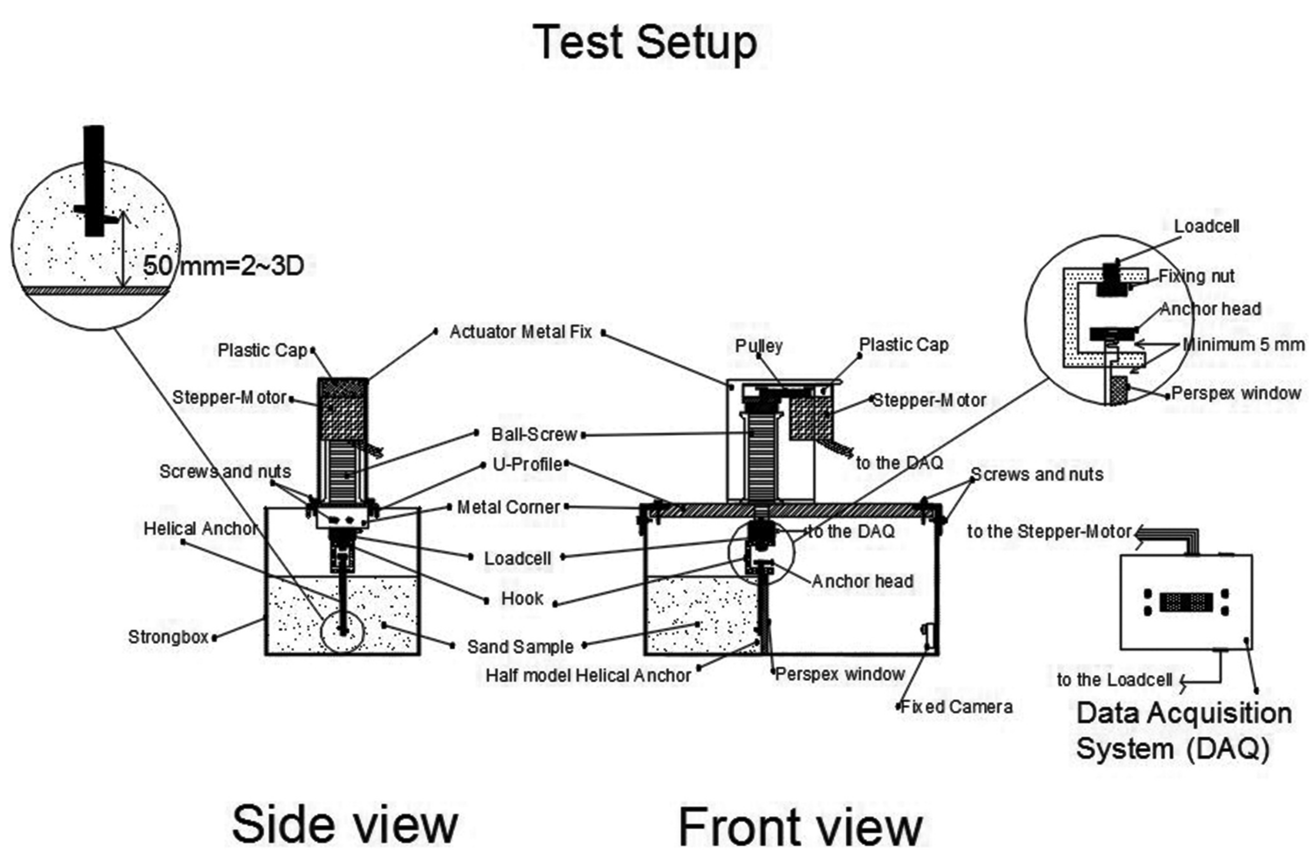

Figure 2. Schematic test setup.

Table 2. Specifications of the tests.

Test case	Shaft diameter (d) (mm)	Prototype shaft diameter (mm)	Helix diameter (D) (mm)	Prototype helix diameter (mm)	WR (D/d)	Embedment depth ratio (H/D)	Helix embedment depth (H) (mm)	Helix pitch (mm)	Helix thickness (mm)	g-level (g)
HA-W2-H3	8	120	16	240	2	3	48	4	1.2	15
HA-W2.5-H3	8	120	20	300	2.5	3	60	4	1.2	15
HA-W3-H3	8	120	24	360	3	3	72	4	1.2	15
HA-W2-H5	8	120	16	240	2	5	80	4	1.2	15
HA-W2.5-H5	8	120	20	300	2.5	5	100	4	1.2	15
HA-W3-H5	8	120	24	360	3	5	120	4	1.2	15

density distinct from that of the rest of the model. The variation in sand relative density during installation is governed by its initial state; dense sand tends loosen within the disturbed zone, whereas loose sand may densify (Sharif, Brown, et al. 2021).

In this study, because the sand was initially in a medium-dense state, a substantial reduction in sand density due to installation was not expected, consistent with observations reported by (Sharif, Brown, et al. 2021). The use of weaker materials to replicate installation disturbances has also been successfully applied by previous researchers, including (Garakani and Maleki 2020; Pérez et al. 2018) and (Salehzadeh, Nuri, and Rafsanjani 2022).

The change in sand density was simulated by pluviating the sand adjacent to the model anchor, referred to as the disturbed area, at a lower relative density than the rest of the model. This was accomplished by pluviating the sand from a reduced height using a half-cut tube and funnel. The pluviation was carried out in 2 cm increments to ensure consistent relative density across the depth. The diameter of the disturbed area was set to 1.2D (where D is the helix diameter), in accordance with observations reported in previous studies Nagai, Tsuchiya, and Shimada (2018), Pérez et al. (2018) and Salehzadeh, Nuri, and Rafsanjani (2022).

While this method of accounting for installation effects may not fully replicate the actual soil behaviour during anchor installation, it is considered sufficiently accurate for observing the failure mechanism, since the elevated gravity within the centrifuge generates vertical and consequently, lateral stresses comparable to those in actual installation conditions. The load response of the anchors, however, may be softer than expected, exhibiting smaller peak capacities compared to a similar soil under real installation conditions. This difference in peak capacity and hence, softer response was documented in a prior study by the authors (Salehzadeh, Nuri, and Rafsanjani 2022) which reported nearly a 10% reduction in peak uplift capacity for the half-model load–displacement curve compared to the full-model curve. Notably, this discrepancy may be more pronounced in denser sands, as the difference in initial lateral in-situ stresses between the two cases becomes more significant.

The half-cut tube was carefully withdrawn vertically after the pluviation process. Coloured sand was placed around the Perspex sheet to enhance visualization of the failure surface. Once the models were prepared, they were pulled out at the target centrifugal acceleration. This process was repeated with different fall heights, and the optimal fall height for preparing the half-models was determined by comparing the resulting load–displacement curves with those of the corresponding full-models, as reported in Heshmati Rafsanjani, Salehzadeh, and Nuri (2021).

It should be noted that the full-models in the referenced study were installed under pitch-matched conditions. Comprehensive details of the physical modelling procedures and verification results are provided in (Salehzadeh, Nuri, and Rafsanjani 2022) and are therefore not repeated here. The connection setup is shown in Figure 3.

Results and discussion

WR effect on the failure mechanism

The effect of WR on the vertical soil deformation contours is shown in Figure 4 for all models, as obtained through PIV analyses. A summary of the observations derived from the PIV analysis is presented in Table 3. As shown in the table, none of the deeply embedded anchors (H/D = 5) exhibited a shallow failure mode, confirming that H/D = 5 corresponds to deep embedment in medium-dense sand, in agreement with the observations of (Al Hakeem and Aubeny 2019; Liu, Liu, and Zhu 2012) and (Salehzadeh, Nuri, and Rafsanjani 2022).

Table 3 also indicates that helical anchors with deep embedment (H/D = 5) exhibit a flow-around failure mechanism, regardless of the WR. This behaviour arises because the force needed to uplift the soil overlying the helix exceeds the force required to shear the soil locally, leading to the formation of the flow-around mechanism (Hossain et al. 2005). The reason for this phenomenon can

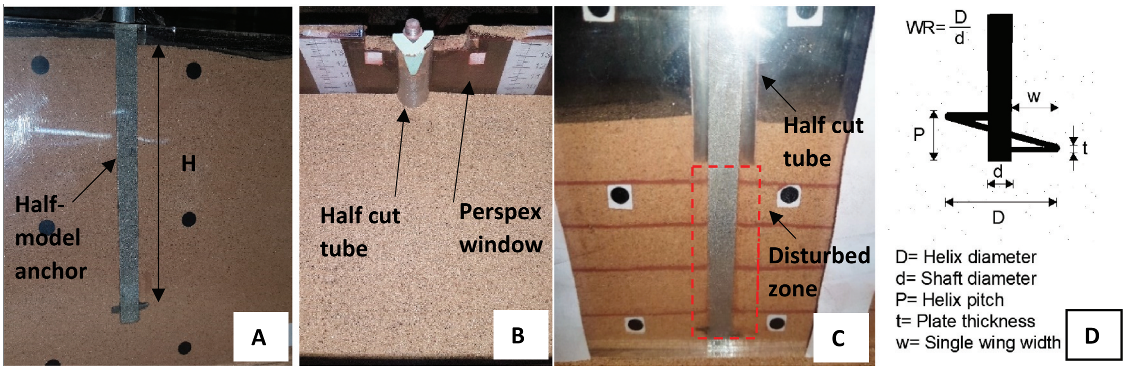

Figure 3. A)Embedded anchor, B) pluviated model and half-cut tube, C) pluviated disturbed zone, D) anchor geometry parameters.

be attributed to two factors: First, as the sand density decreased due to the installation process, the force required for the flow-around mechanism also decreased. Second, as the embedment depth increased, the confining stress and the required uplift force increased. These conditions favour local shear (deep failure) over general shear failure (shallow failure). It is worth noting that these failure mechanisms can be observed through the total displacement fields around the anchors, as presented in Figure 5.

Further, according to Table 3, in the shallow embedment cases, general shear failure characterized by a reversed truncated cone failure zone was the dominant mechanism, as expected. In the deep embedment cases, a flow-around failure mechanism was observed. All models exhibited the anticipated failure mechanisms, except for the HA-W3-H3 model. For this model, which had the largest WR and was embedded at H/D = 3 (shallow embedment), a flow-around mechanism was observed, even though the failure surface reached the ground level, indicating a shallow failure mode. A close-up view of the total displacement vector field for HA-W3-H3 model is shown in Figure 6.

This is intriguing, as the flow-around failure mechanism is typically associated with deep embedment failure modes, while the extension of the failure surface to the ground level is linked to shallow failure modes. The failure mechanism observed in the HA-W3-H3 model clearly differs from both deep and shallow failure modes, suggesting a hybrid or combined failure mechanism representative of an intermediate embedment depth, indicating a transitional failure mode.

This is likely due to the single wing width (W) of the HA-W3-H3 model, which, combined with the largest WR, can mobilize a larger soil volume compared to other tested models, while its relatively shallow embedment depth facilitates uplift of the overlying soil. This transitional failure mechanism can potentially be attributed to changes in overburden stresses and the principle of energy minimization.

On the one hand, as WR increased, the embedment depth (H) would also increase to maintain the embedment ratio at H/D = 3. The increased embedment (H) raises confining stress levels which can suppress soil movement to the surface and promote localized soil displacement (flow-around mechanism). On the other hand, large effective diameter (W) and hence bearing area of the plate has the potential to lift a substantial soil volume, especially since embedment depth remains shallow. Given the embedment is considered as shallow (H/D = 3), the soil wedge can still reach the soil surface, and hence the attributes of shallow failure mechanism become evident.

Another mechanism that could contribute to a combined failure mechanism is the energy minimization, as mentioned by (Hossain et al. 2005) which outlines that failure mechanisms develop in a way that minimize total work (or energy requirements). In cases where different failure mechanisms require comparable energy levels to develop, the minimum-energy governing failure mechanism may not develop easily, and transitional failure mechanisms may occur such as that observed for HA-W3-H3 model (H/D = 3, WR = 3).

Therefore, while characteristics of both failure mechanisms can be observed in this scenario, this failure mechanism might not be categorized strictly as shallow or deep; it represents a transitional failure mechanism. It is likely that the energy required to mobilize either failure mechanisms (shallow or deep) would be comparable in this case, generally depending on soil conditions and anchor geometry including soil density, in-situ stresses, anchor wing ratio (WR) and embedment depth (H/D).

Figure 5 presents the displacement vector field for the anchors, illustrating the described failure mechanisms. It is evident that the flow-around mechanism remains largely unaffected by variations in WR in the deep embedment cases. In contrast, for shallow embedment modes, a potential relationship between

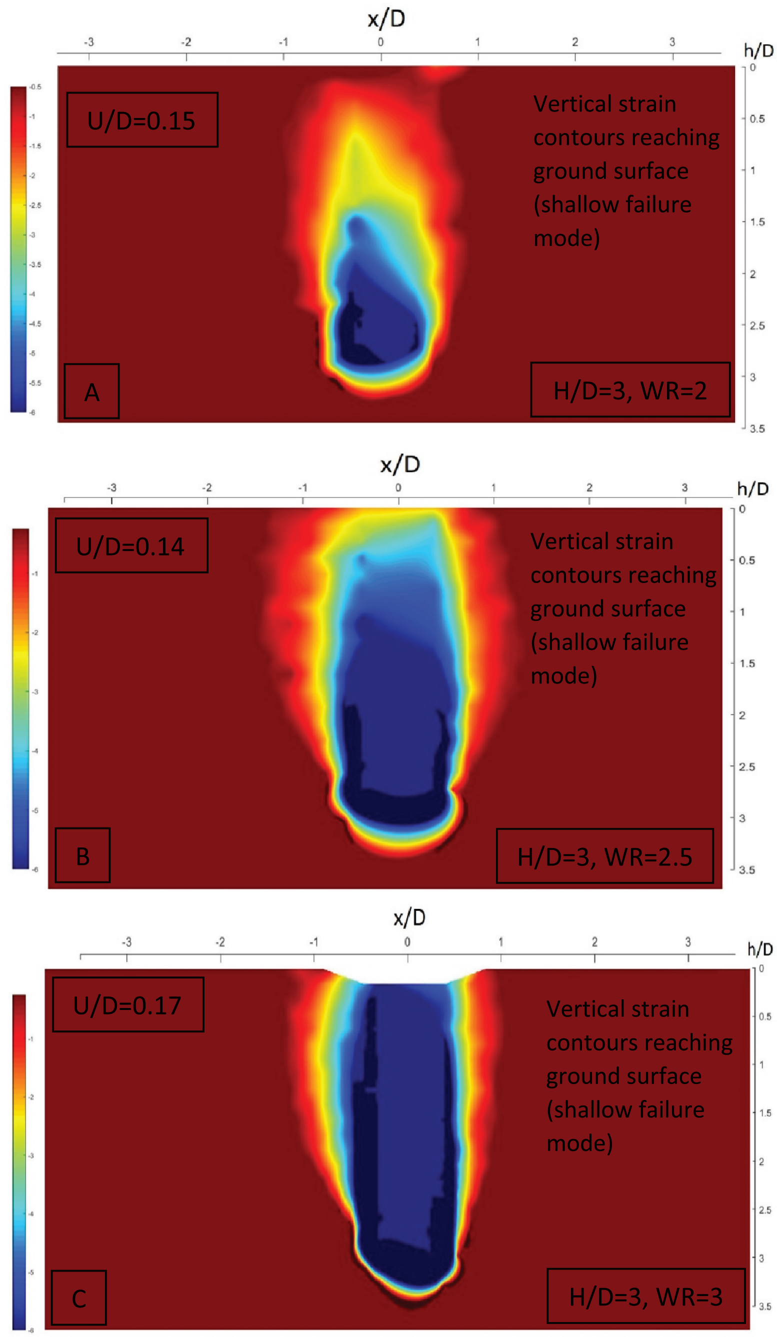

Figure 4. Vertical strain contours of the anchors obtained through PIV analysis.

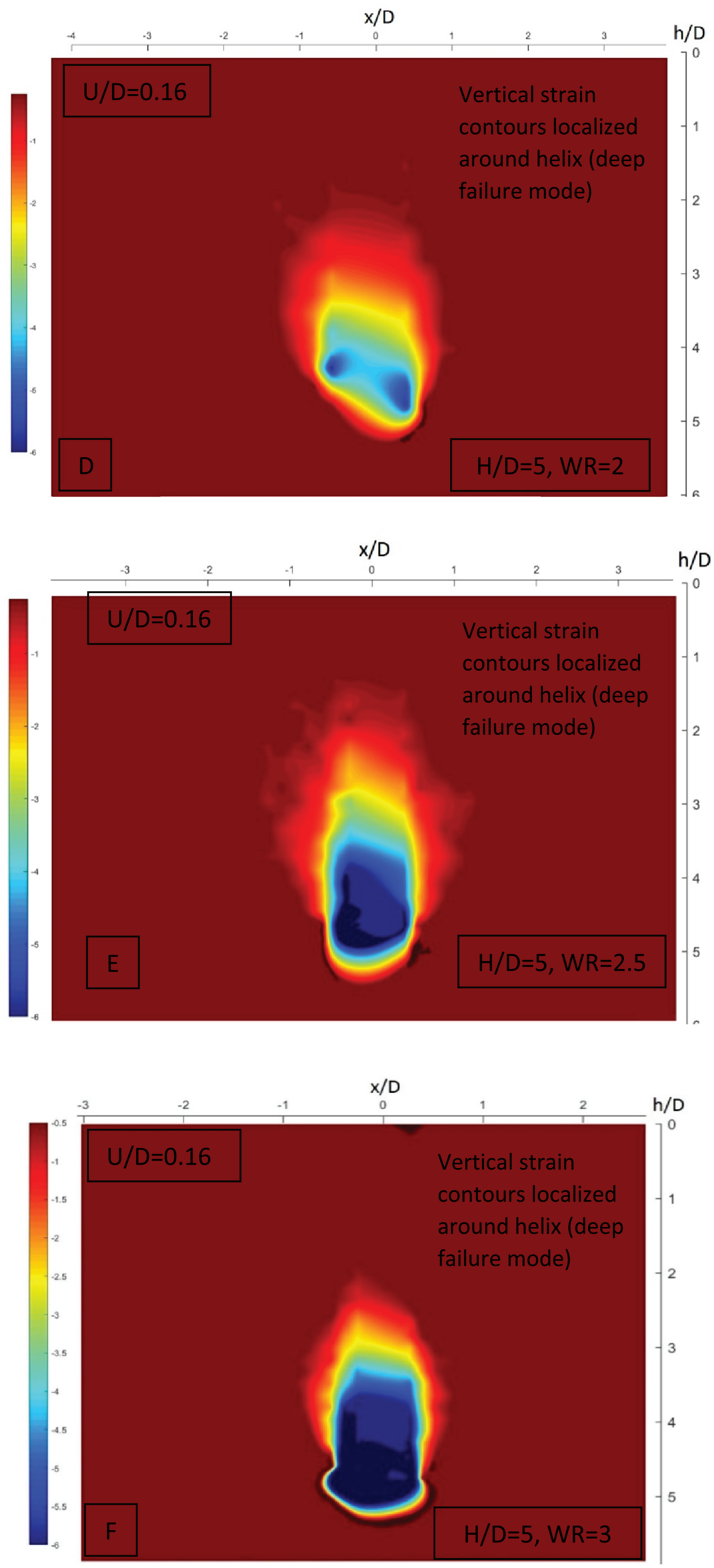

Figure 4. (Continued).

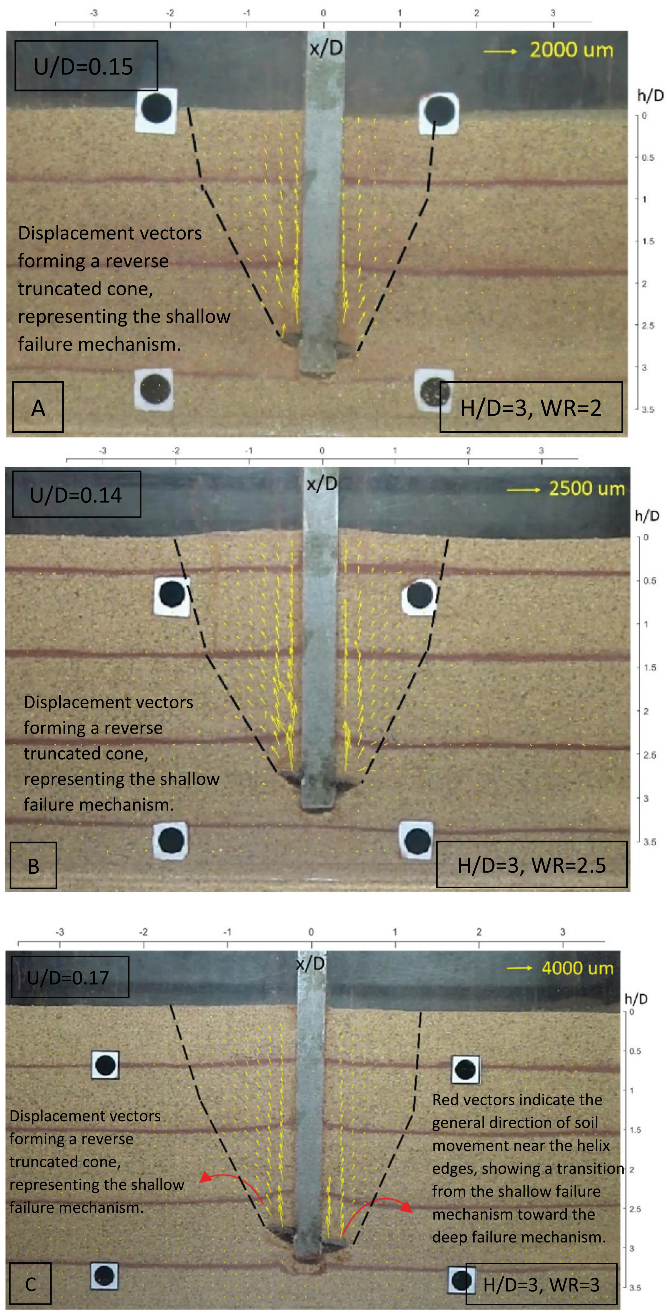

Figure 5. Total displacement field and failure mechanism of the anchors. (U: anchor head displacement, D: helix diameter).

WR and the critical embedment depth may exist, as discussed previously. Further investigation is needed to establish any definitive relationship between WR, changes in the failure mechanism, and the critical embedment depth.

Another key observation is the change in the failure mechanism with increasing embedment ratio. As the embedment ratio increased from H/D = 3 to H/D = 5, the failure mechanism shifted from general shear failure to the flow-around failure mode. This trend is consistent with the findings of previous studies, including Al Hakeem and Aubeny (2019); Liu, Liu, and Zhu (2012); Zhang (1999) and Ilamparuthi, Dickin, and Muthukrisnaiah (2002).

WR effect on the uplift capacity and pressure

The results of the peak uplift capacity (maximum load achieved during testing) of the anchors are presented in Table 4. The measured load values for

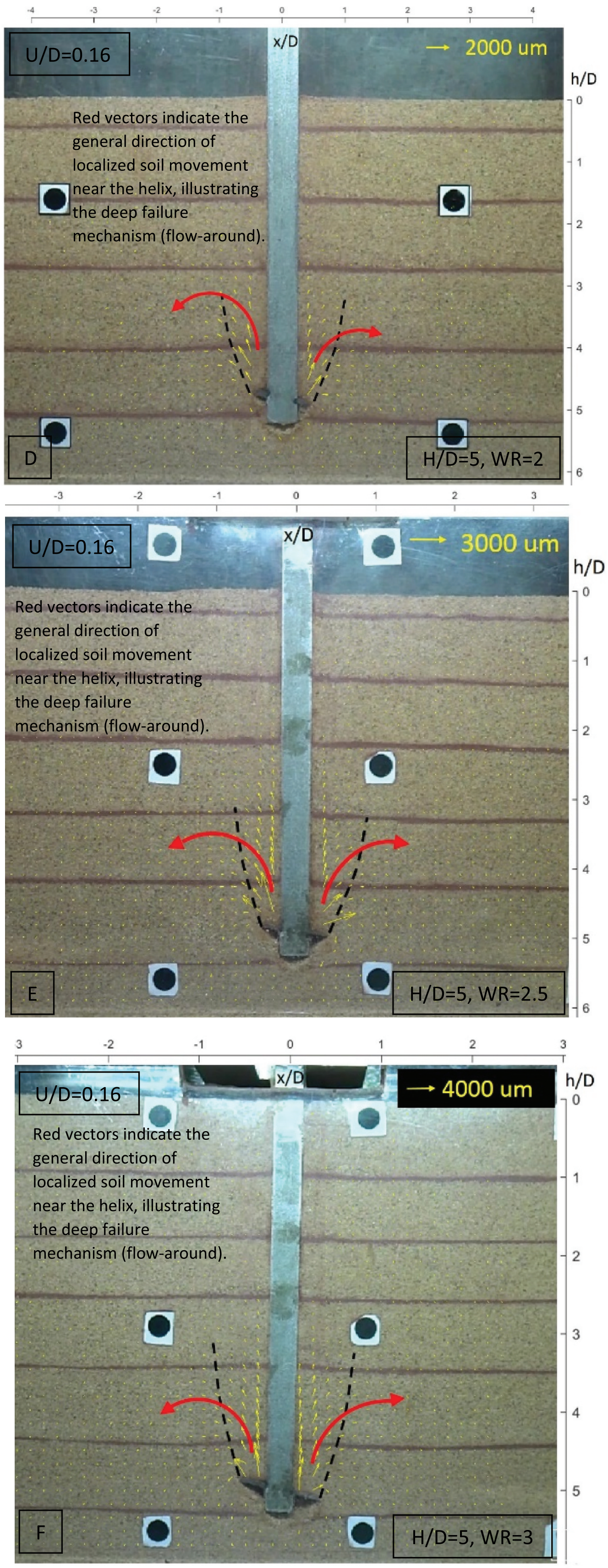

Figure 5. (Continued).

Table 3. Summary of the PIV analysis results.

Model case	WR (D/d)	Embedment depth ratio (H/D)	Failure surface extension to the soil surface	Flow-around mechanism
HA-W2-H3	2	3	Yes	No
HA-W2.5-H3	2.5	3	Yes	No
HA-W3-H3	3	3	Yes	Yes
HA-W2-H5	2	5	No	Yes
HA-W2.5-H5	2.5	5	No	Yes
HA-W3-H5	3	5	No	Yes

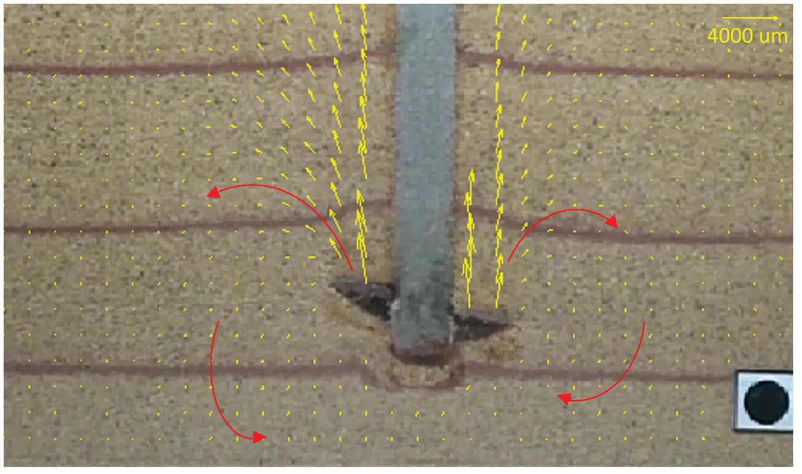

Figure 6. Close-up view of the HA-W3-H3 model (WR=3, H/D=3).

all tests were doubled to account for the halved helix and shaft, ensuring comparability with the existing literature. According to Table 4, the peak uplift capacity of the anchors generally increased with an increase in helix diameter, as the embedment ratio increased across different WRs, similar to the trend observed in Garakani and Maleki (2020) and Tsuha et al. (2012).

A more detailed investigation into the effect of WR on the uplift capacity can be achieved by examining the peak helix pressure of the anchors. Because the peak uplift capacity (force) generally increases with the helix diameter, the peak helix pressure provides a more accurate measure of the load-bearing efficiency of the helices. The peak helix pressure, presented in Figure 7, is calculated by dividing the peak uplift force by the net projected area of the helix.

According to Figure 7, the peak helix pressure decreased as the WR increased for both deep and shallow embedment depths, with the rate of decline being similar in both cases. This reduction in peak helix pressure is attributed to the larger disturbed zone in the sand. A larger WR corresponds to a greater volume of sheared sand and reduced density, as observed in pitch-matched installations by (Sharif et al. 2021). Consequently, increasing the WR results in greater soil disturbance, lower relative density in the sand, and a corresponding decrease in the peak helix pressure of the anchors.

A similar observation was reported by da Silva and Tsuha (2021) in their calibration chamber tests on prototype helical anchors. Nagata and Hirata (2005) also documented a similar trend in their 1 g tests on small-scale helical anchors. Additionally, as shown in Figure 7,

Table 4. Measured peak uplift capacity, pressure and sand density (prototype scale).

Model case	WR (D/d)	Embedment depth ratio (H/D)	Unit weight (kN/m^3)	Relative density (%)	Peak uplift capacity (kN)	Peak helix pressure (kPa)
HA-W2-H3	2	3	15.77	64	8.3	246
HA-W2.5-H3	2.5	3	15.72	63	13.1	221
HA-W3-H3	3	3	15.68	61	17.2	191
HA-W2-H5	2	5	15.51	56	11.8	349
HA-W2.5-H5	2.5	5	15.76	64	20.1	338
HA-W3-H5	3	5	15.73	63	27.5	304
Average	–	–	15.69	62%	–	–

the peak helix pressure clearly increased with increasing embedment depth for a given WR. This increase is due to the higher uplift capacity resulting from greater overburden pressure, while the projected area of the helix remained constant.

Figure 8 presents the dimensionless breakout factor N_{qu} for the performed tests. The dimensionless breakout factor is commonly used to estimate the ultimate uplift capacity of helical anchors and embedded plates and is calculated using equation (1):

$$N_{qu} = \frac{Q}{\gamma' H A_h} \quad (1)$$

Where: Q is the peak uplift capacity of the helical anchor (kN), γ' is the effective unit weight of the soil (kN/m^3), H is the embedment depth (m) and A_h is the net projected helical plate area (m^2).

According to Figure 8, the dimensionless breakout factor N_{qu}, is influenced mainly by the WR of the helical anchors, with a relatively smaller effect from embedment depth ratio. Figure 8 illustrates that N_{qu} decreased substantially as WR increased, regardless of the failure mode or embedment depth. This observation somewhat contrasts the prevailing understanding in the literature, which suggests that N_{qu} depends solely on the soil friction angle and embedment depth and is independent of anchor geometry. Further research is necessary to validate and improve understanding of the effect of anchor geometry on N_{qu}.

This observation suggests that while N_{qu} is generally considered to be influenced mainly by soil friction angle (Φ) and embedment depth (H/D) for most anchor types including helical anchors, a third parameter, wing ratio (WR), might also affect N_{qu}. A potential explanation for this influence of WR is that the annular disturbed soil zone above the helix which governs the anchor capacity, increases in size with increasing WR. This leads to a greater reduction in radial stresses and consequently, a more pronounced reduction in both anchor uplift capacity and N_{qu}. It is noted that radial stresses were not measured in the present study, however, such a relationship between WR and anchor uplift performance was reported in (da Silva and Tsuha 2021) through measurements of soil lateral stresses in calibration chamber tests on model helical anchors.

Another reason why WR may influence the capacity of helical anchors (in addition to soil friction angle (Φ), and embedment depth H/D, which are typical influencing factors for most anchor types) is the higher levels of soil disturbance induced during installation of helical anchors in sand. The extent and size of this disturbed zone depend on anchor geometry, particularly the helix and shaft diameters, which are collectively expressed through WR. Larger WR values are associated with greater disturbance, leading to reduced uplift resistance and lower values of both N_{qu} and bearing capacity of the anchors. Therefore, WR should be considered as an additional design parameter when evaluating helical anchors for uplift loads. This consideration becomes especially critical when anchors are intended to resist large tensile forces, such as mooring loads applied by tension leg platforms (TLPs) in offshore environments.

It is noted that overflighting has been introduced as an alternative installation method (Cerfontaine et al. 2023) to reduce soil disturbance to improve the anchor capacity and reduce installation torque compared with the traditional pitch-matched installation method.

Another noteworthy observation from Figure 8 is that the influence of embedment depth on the N_{qu}

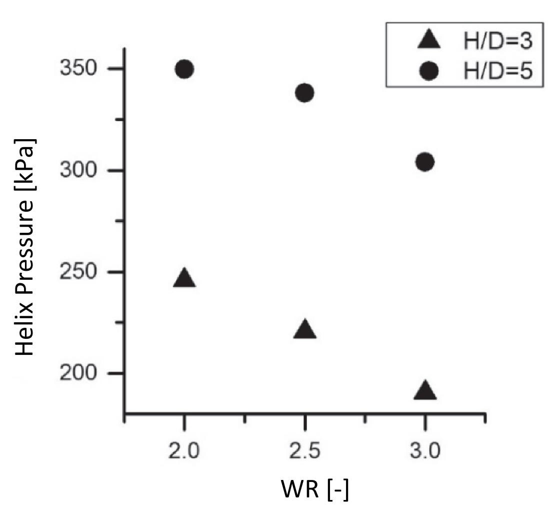

Figure 7. Peak helix pressure and WR of the tests.

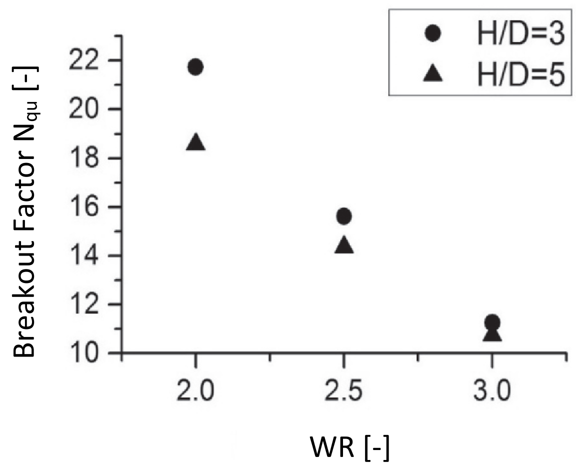

Figure 8. Breakout factor N_{qu} and WR of the tests.

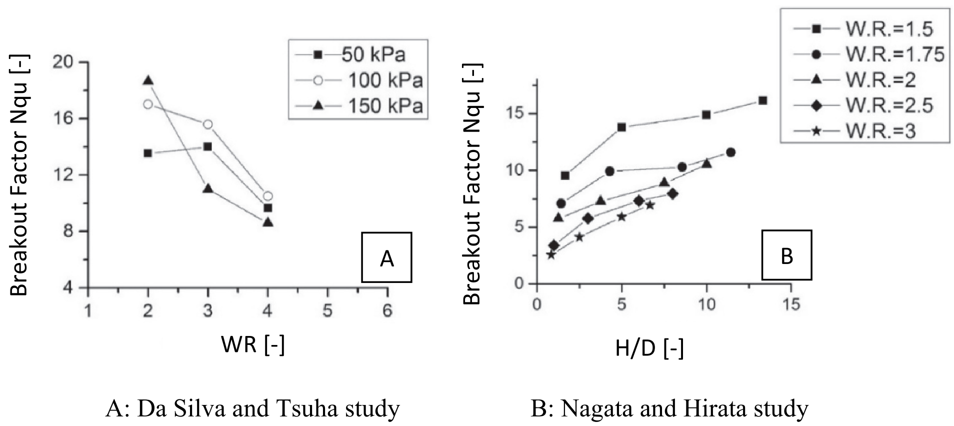

Figure 9. Breakout factor N_{qu} and WR correlation for previous studies.

factor diminished as the WR increased. For instance, at WR = 2, the difference in N_{qu} between shallow and deep modes was 17%, whereas this difference decreased to only 4% when WR increased to 3. This trend suggests that for larger WRs, the N_{qu} factor likely converges to similar values across different embedment depths, unlike higher variation observed at smaller WRs.

This observation was further corroborated by the results of tests on helical anchors reported by (da Silva and de Tsuha 2021), where monotonic uplift tests were performed on prototype models with varying WRs. Their findings demonstrated a decline in peak uplift pressure with increasing WR, however, the study did not explicitly examine the N_{qu} factor. Subsequent calculations of N_{qu} based on their experimental data revealed a comparable trend: N_{qu} values corresponding to different embedment ratios (represented by vertical surcharges in this case) progressively converged as WR increased from 2 to 4, as illustrated in Figure 9a. Notably, a significant reduction in N_{qu} by 30–50% was observed as WR increased from 2 to 4.

This finding offers valuable insight into the discrepancies in N_{qu} factors reported across various studies in literature. The potential dependency of N_{qu} on WR needs further in-depth investigation to advance the understanding of this critical aspect of helical anchor design and analysis. Again, it is essential to underscore that N_{qu} is distinct from the peak helix pressure, despite both parameters exhibiting a similar decreasing trend with increasing WR.

The correlation between the WR and N_{qu} factor was further investigated by verifying it against the experimental results reported by Nagata and Hirata (2005). These authors conducted calibration chamber tests on medium-scale models, from which N_{qu} factors were derived based on the test specifications and experimental outcomes, as presented in Figure 9b. As shown, the N_{qu} factor exhibited a consistent decline with increasing

WR in their study, further reinforcing the observed relationship between WR and N_{qu}.

The reduction in N_{qu} observed in (Nagata and Hirata 2005) as WR increased from 2 to 3 was particularly noteworthy. It is important to highlight that a decreasing correlation between plate diameter and N_{qu} factor was previously reported by (de Hollanda Cavalcunti Tsuha et al. 2019). However, the reductions in N_{qu} factors reported in that study were moderate, amounting to approximately 20% in dense sand and 30% in medium-dense sand for anchors with comparable D/d and H/D ratios. These findings underscore the potential significance of WR in influencing the breakout factor of helical anchors. Further research is essential to provide a deeper understanding of the influence of WR on the N_{qu} factor and its implications for anchor design and analysis.

WR effect on the formed gaps and displacement fields

The horizontal displacement contours around the anchors at peak uplift load are presented for two models in Figure 10. A summary of the observations and measurements is also given in Table 5. The influence distance of the failure surface in vertical directions is determined by considering a minimum threshold strain. This minimum strain was taken at 0.5% to account for small movements within samples due to anchor pullout. For horizontal influence distance, however, a maximum strain of ±3% was considered. It should be noted that choosing smaller strain threshold values would have captured very small movements within the soil mass which might not represent the actual influenced zone. According to Table 5 and Figure 10, in the deep failure conditions (H/D = 5), as the helix diameter and WR increased, the normalized horizontal influence zone around the anchor (at the peak uplift load) decreased. This is probably because the effective vertical and lateral earth pressure increased with the increase of the helix diameter (to maintain H/D = 5) and therefore, the increased confining pressure prevented further expansion of influence zone.

In the shallow mode of failure (H/D = 3), this trend was reversed. As the WR and helix diameter increased, the extent of the lateral influence zone increased. The normalized vertical influence zone (vertical strain contours are shown in Figure 4) was similar (= 3D) for all shallow anchors because of the limited embedment depth. However, the normalized horizontal influence zone ranged from 1.5D to 2.4D as the WR increased from 2 to 3. A similar influence zone was observed in the results of Sharif, Brown, et al. (2021). These authors simulated screw pile tensile loading in different sand densities using discrete element method (DEM). The results indicated that the soil was influenced by a distance of 2D and 3D from the pile vertical axis for the deep and shallow modes of failure, respectively (pitch-matched installation). These authors tested screw piles with WR = 2 only.

The difference in influenced zone extent between the shallow and deep modes was due to different failure mechanisms. In the deep mode, the dominating failure mechanism was the flow-around mechanism, while in the shallow mode, the general shear failure (or reversed truncated cone failure) prevailed. This observation emphasizes the importance of proper failure mechanism detection for valid consideration of the interaction of adjacent anchors.

The sequence of gaps development and influencing parameters are of interest for evaluating cyclic performance. An experimental study by (Urabe et al. 2015) indicated that gaps presence and infilling affect the cyclic axial performance of the anchors during compressive/tensile loading, mainly due to presence of disturbed soil above/beneath the plate. The gaps infilling was also suggested to be influenced by anchor WR and wing area.

In a separate study, Schiavon et al. (2019) commented that gap development depends on the accumulated displacement (U_{acc}) to d_{50} (U_{acc}/d_{50}). The ratio of monotonic uplift displacement to the average diameter of soil particles (U/d_{50}) was studied in the current research to provide insight into the development of gaps beneath the anchor for future studies.

At the start of the test, the gaps were not present beneath the test anchors since no uplift occurred. After certain uplift displacement, three separate gaps developed beneath the wings and the anchors' shaft. The gaps' size began to grow until formed voids started to fill. It is noteworthy that the gaps never were filled completely because of the constant pulling and absence of cohesion or suction within the tested sand.

The formed gaps for WR = 2 and WR = 3 are shown for different embedment in Figure 11. It is interesting to note that the height of the gaps beneath the wings was dependent on WR; as the WR increased, the gap height also increased. A geometrical correlation was also observed for the average gap height. For WR = 2, the average gap height beneath the two edges of the helix was almost $6d_{50}$, while this was $12d_{50}$ for WR = 3. The WR = 2 had a single wing width ($\frac{D-d}{2}$) of 4 mm, while WR = 3 had a single wing width of 8 mm. The results of the average gap height and single wing width for all models are presented in Table 6. Therefore, the average gap height (G) was on average 40% (4/10) of the single

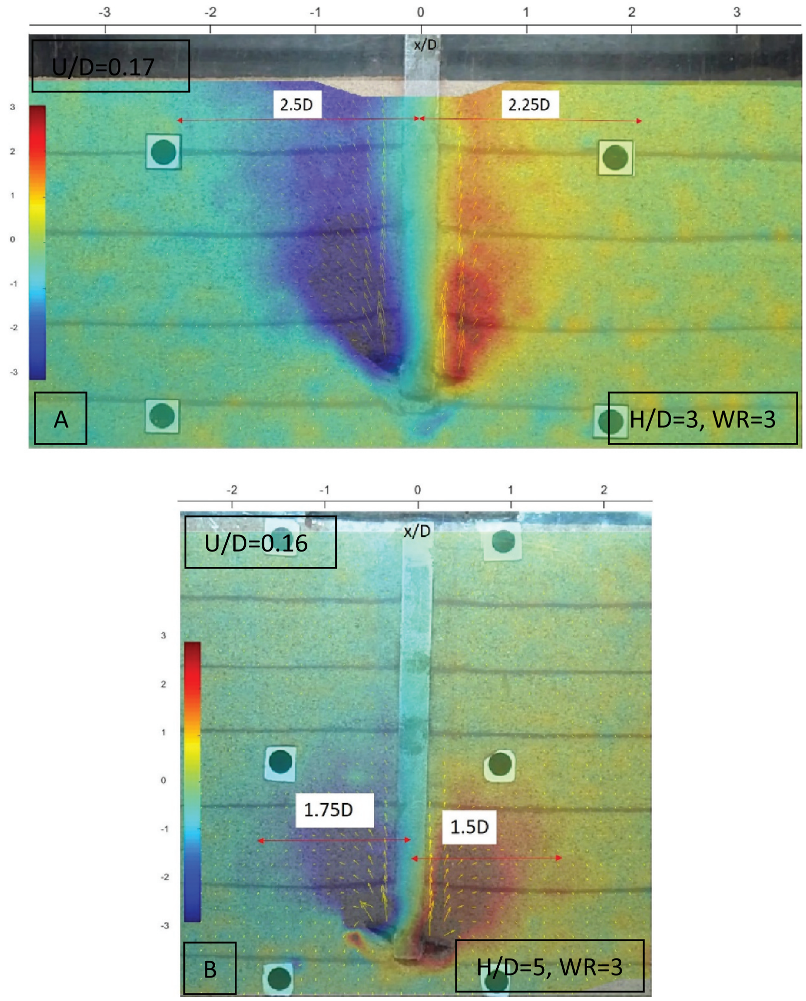

Figure 10. Horizontal strain contours at peak uplift load for two models: a)HA-W3-H3, b) HA-W3-H5.

Table 5. Summary of the observations through PIV analysis.

Model case	WR (D/d)	Embedment ratio (H/D)	Failure surface vertical influence distance (D:helix diameter)	Failure surface horizontal influence distance	$(U/D)_{peak}$	$(U/d_{50})_{infilling\ initiation}$
HA-W2-H3	2	3	3D	1.5D	0.15	6.2
HA-W2.5-H3	2.5	3	3D	1.9D	0.14	9.8
HA-W3-H3	3	3	3D	2.4D	0.17	13.1
HA-W2-H5	2	5	3.25D	2.1D	0.16	5.5
HA-W2.5-H5	2.5	5	3.5D	1.75D	0.16	8.2
HA-W3-H5	3	5	2.75D	1.6D	0.16	10.9

wing width in the current study and it did not have a unique relationship with either WR or the embedment ratio (H/D). It should be noted that the observed correlation between the average gap height and WR is specific to the tested sand and may not be used for other soil types without proper verification.

The gaps start to fill at different normalized displacements. Table 5 Indicates the required displacement to initiate gaps filling (U/d_{50}) for tested anchors. It should be noted that the presented U/d_{50} values indicate the displacement required for the constant flow of the sand particles into the gap, i.e. angle of repose of the sand in the gaps' base reaches a constant value which is close to the critical state friction angle (φ_{cs}) of the tested sand (see Table 1).

According to Table 5, the U/d_{50} increased with increasing WR while it decreased with increasing H/D. The reason for the U/d_{50} increase with the WR is that with larger WR, the created voids beneath the helix are larger and thus, more sand particles from above and around the helix are required to fill the gaps, meaning that the helix can move more freely in the pulling

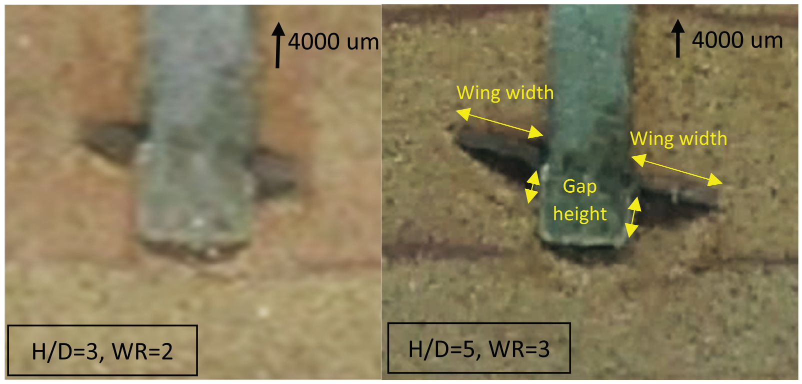

Figure 11. Formed gaps beneath HA-W2-H3 (left) and HA-W3-H5 (right).

direction. This resulted in increased required displacement to fill the gap with increased wing length and WR.

It is also believed that the reverse correlation of U/d_{50} with the embedment ratio was the result of increased overburden pressure which in turn pushed the sand particles to fill the gaps at smaller displacements. Schiavon et al. (2019) tested helical anchors and reported that gaps were filled at different displacements for different d_{50} of the sand. Schiavon, Tsuha, and Thorel (2017) performed cyclic loading tests on centrifuge models of helical anchor and reported that formed gaps were quickly filled with sand grains due to the cyclic movement of the helix. They suggested that the formed gap would have filled earlier and the anchor response would be less stiff, had the sand d_{50} been smaller (because of reduced lateral pressure). Therefore, it can be concluded that gap size and the required displacement to fill the gaps depends on the WR and embedment depth of the helix in addition to the d_{50} of the soil.

Conclusions

A total of 6 centrifuge tests were performed on model helical anchors installed in medium-dense sand to evaluate the effect of WR on the failure mechanism and uplift performance of the anchors. The installation disturbance was simulated by a novel technique that reproduced the density change but did not capture the stress redistribution, which are both the results of installation disturbance. The main findings of this study include:

- The failure mechanism in the deep failure mode ($H/D = 5$) was a flow-around mechanism regardless of the WR of the anchor. In the shallow mode ($H/D = 3$), the failure mechanism was reversed truncated cone; although the failure mechanism changed to a combination of reversed truncated cone and flow-around mechanism at $WR = 3$ in this mode, resulting in a flow of soil particles around the helix near the ground surface. This was probably due to the large wing of the model that mobilized a large soil mass while the small embedment of the helix made it easy to uplift the soil overlying the helix.
- The uplift capacity of the anchors increased with increasing the embedment depth and WR. Though the peak helix pressure (defined as peak uplift capacity/helix surface area) reduced with increased helix diameter and WR. This is attributed to the larger disturbed zone in the soil above the helix as a result of installation. This indicates
- The dimensionless breakout factor N_{qu} had a declining correlation with WR and this was true in both shallow and deep embedment conditions. This observation was also verified for other studies and a similar trend was noticed. This is rather different from the previous perception that N_{qu} factor is only dependent on the helix embedment

Table 6. Summary of observations through PIV analysis.

Model case	WR (D/d)	Average gap height (G)	Single wing width (mm) $(\frac{D-d}{2})$	$\left(\frac{G}{\frac{D-d}{2}}\right)$ Ratio
HA-W2-H3	2	$6\times d_{50}$ (1.5mm)	4	0.37
HA-W2.5-H3	2.5	$10.5\times d_{50}$ (2.65mm)	6	0.44
HA-W3-H3	3	$12\times d_{50}$ (3mm)	8	0.37
HA-W2-H5	2	$6.5\times d_{50}$ (1.6mm)	4	0.40
HA-W2.5-H5	2.5	$10\times d_{50}$ (2.55mm)	6	0.43
HA-W3-H5	3	$12\times d_{50}$ (3.1mm)	8	0.38

depth ratio and friction angle of the soil. Further tests are required to fully capture the effects of WR on N_{qu} and improve analytical prediction of anchors uplift capacity with consideration of anchor geometry.

- The large disturbed sand area above the helices (due to installation) which gets even larger with higher WR ratios could mean larger WRs do not necessarily improve uplift capacity efficiency of the anchors. This requires further attention when designing these anchors to withstand large uplift mooring loads (such as those applied through TLP mooring lines)
- The dimensionless uplift distance required to fill the gaps (U/d_{50}) increased with increasing WR and decreasing embedment depth. The reasons for such observation were larger helix, resulting in a wider gap beneath the helix, and increased embedment, resulting in higher confining and lateral pressures and thus, more pushing force behind the particles to fill the gaps. The gaps infilling can influence the cyclic capacity and accumulated displacements of the anchors and understanding of how the infilling develops beneath the anchors can improve design of the anchors to withstand large vertical cyclic loads.
- The influence zone around the helix in the horizontal direction was affected by the WR and embedment depth. In the shallow failure mode, increasing the WR resulted in an extension of the horizontal influence zone while in the deep mode, the horizontal influence zone shrank as the WR increased. Furthermore, the average ratio of gap height to single-wing width $\left(\frac{G}{\frac{D-d}{2}}\right)$ was nearly 40% in the current study, irrelevant of the WR or H/D. Understanding the influence zone around the anchors can improve the design of helical anchor groups by optimizing their distance to minimize interaction and improve individual bearing capacities.

Availability of data and material

The data and material presented here is available upon request from the corresponding author.

Code availability

GeoPIV-RG code which is a free MATLAB code was used in preparing the PIV analysis results of this research.

Disclosure statement

No potential conflict of interest was reported by the author(s).

Funding

The authors declare that no funding was received to perform this research.

ORCID

Hamed Nuri http://orcid.org/0000-0003-4332-7575
Hossein Salehzadeh http://orcid.org/0000-0003-0289-6640
Ali Akbar Heshmati Rafsanjani http://orcid.org/0000-0002-2681-2280
Cristina de Hollanda Cavalcanti Tsuha http://orcid.org/0000-0001-7543-9083
Amin Askarinejad http://orcid.org/0000-0002-7060-2141

References

Al Hakeem, N., and C. Aubeny. 2019. "Numerical Investigation of Uplift Behavior of Circular Plate Anchors in Uniform Sand." *Journal of Geotechnical and Geoenvironmental Engineering* 145 (9): 04019039. Sep. https://doi.org/10.1061/(ASCE)GT.1943-5606.0002083.

Baziar, M. H., H. Shahnazari, and M. Kazemi. 2018. "Mitigation of Surface Impact Loading Effects on the Underground Structures with Geofoam Barrier: Centrifuge Modeling." *Tunnelling and Underground Space Technology* 80:128–142. Oct. https://doi.org/10.1016/j.tust.2018.06.010.

Brown, M. J. 2019. "Screw Pile Research at the University of Dundee." In *1st International Symposium on Screw Piles for Energy Applications*, 1–13. University of Dundee.

Brown, M. J., C. Davidson, B. Cerfontaine, M. Ciantia, and J. Knappett. 2019. "First Indian Symposium on Offshore Geotechnics (ISOG 2019) Developing Screw Piles for Offshore Renewable Energy Application." First Indian Symposium on Offshore Geotechnics (ISOG 2019), Indian Institute of Technology Bhubaneswar (IIT-BBS), India, 1–9.

Cerfontaine, B., M. J. Brown, J. A. Knappett, C. Davidson, Y. U. Sharif, M. Huisman, M. Ottolini, and J. D. Ball. 2023. "Control of Screw Pile Installation to Optimise Performance for Offshore Energy Applications." *Geotechnique* 73 (3): 234–249. https://doi.org/10.1680/jgeot.21.00118.

Cerfontaine, B., C. Davidson, M. J. Brown, J. A. Knappett, and Y. U. Sharif. 2020. "Centrifuge Testing of Large Screw Pile Geometries for Offshore Applications." Proceedings of the Piling 2020 Conference, 139–144. University of Durham, UK: ICE Publishing. Jan. https://doi.org/10.1680/egip.63631.121.

Chen, Y., A. Deng, F. Lu, and H. Sun. 2020. "Failure Mechanism and Bearing Capacity of Vertically Loaded Pile with Partially-Screwed Shaft: Experiment and Simulations." *Computers and Geotechnics* 118 (November 2019): 103337. https://doi.org/10.1016/j.compgeo.2019.103337.

Chen, Y., A. Deng, A. Wang, and H. Sun. 2018. "Performance of Screw–Shaft Pile in Sand: Model Test and DEM

Simulation." *Computers and Geotechnics* 104 (August): 118–130. https://doi.org/10.1016/j.compgeo.2018.08.013.

da Silva, D. M., and C. D. H. C. Tsuha. 2021. "Experimental Investigation on the Installation and Loading Performance of Model-Scale Deep Helical Piles in Very Dense Sand." *Canadian Geotechnical Journal* 58 (9): 1379–1395. Sep. https://doi.org/10.1139/cgj-2020-0317.

Davidson, C., M. J. Brown, A. J. Brennan, J. A. Knappett, B. Cerfontaine, and Y. U. Sharif. 2019. "Physical Modelling of Screw Piles for Offshore Wind Energy Foundations." Proceedings of the 1st International Screw Pile Symposium on Screw Piles for Energy Applications, Dundee, Dundee, Scotland, 31–37.

Davidson, C., M. J. Brown, B. Cerfontaine, T. Al-Baghdadi, J. Knappett, A. BrennanC. Augarde, et al. 2022. "Physical Modelling to Demonstrate the Feasibility of Screw Piles for Offshore Jacket-Supported Wind Energy Structures." *Géotechnique* 72 (2): 108–126. Sep. https://doi.org/10.1680/jgeot.18.P.311.

de Hollanda Cavalcunti Tsuha, C., J. A. Schiavon, L. Thorel. 2019. "Evaluation of the Breakout Factor for Helical Anchors in Sand by Centrifuge Testing." In *Geotechnical Engineering in the XXI Century: Lessons Learned and Future Challenges*, edited by N.P. López-Acosta, 905–912. IOS Press. https://doi.org/10.3233/STAL190128.

Garakani, A. A., and J. Maleki. 2020. "Load Capacity of Helical Piles with Different Geometrical Aspects in Sandy and Clayey Soils: A Numerical Study." *Sustainable Civil Infrastructures* 1:73–84. https://doi.org/10.1007/978-3-030-34178-7_7.

Garnier, J., C. Gaudin, S. M. Springman, P. J. Culligan, D. Goodings, D. Konig, B. Kutter, R. Phillips, M. F. Randolph, and L. Thorel. 2007. "Catalogue of Scaling Laws and Similitude Questions in Geotechnical Centrifuge Modelling." *International Journal of Physical Modelling in Geotechnics* 7 (3): 01–23. Sep. https://doi.org/10.1680/ijpmg.2007.070301.

Ghaly, A., A. Hanna, and M. Hanna. 1991. "Uplift Behaviour of Screw Anchors in Sand. I: Dry Sand." *Journal of Geotechnical and Geoenvironmental Engineering* 117 (5): 773–793. https://doi.org/10.1061/(ASCE)0733-9410(1991)117:5(773).

Giampa, J. R., A. S. Bradshaw, and J. A. Schneider. 2017. "Influence of Dilation Angle on Drained Shallow Circular Anchor Uplift Capacity." *The International Journal of Geomechanics* 17 (2): 1–11. https://doi.org/10.1061/(ASCE)GM.1943-5622.0000725.

Hao, D., D. Wang, C. D. O'Loughlin, and C. Gaudin. 2019. "Tensile Monotonic Capacity of Helical Anchors in Sand: Interaction between Helices." *Canadian Geotechnical Journal* 56 (10): 1534–1543. Oct. https://doi.org/10.1139/cgj-2018-0202.

Hasanlourad, M., S. M. H. Khatami, and M. M. Ahmadi. 2018. "Effect of Bentonite Fine Content on the Triaxial Shear Behavior of Sandy Soils." *AUT Journal of Civil Engineering* 2 (2): 177–182. Dec. https://doi.org/10.22060/ajce.2018.14451.5476.

Heshmati Rafsanjani, A. A., H. Salehzadeh, and H. Nuri. 2021. "Evaluating Scale Effects and Bearing Portions in Centrifuge Modeling of Helical Anchors: Sand." *Acta Geotechnica* 16 (9): 2917–2932. Sep. https://doi.org/10.1007/s11440-021-01156-2.

Hossain, M. S., Y. Hu, M. F. Randolph, and D. J. White. 2005. "Limiting Cavity Depth for Spudcan Foundations Penetrating Clay." *Géotechnique* 55 (9): 679–690. https://doi.org/10.1680/geot.2005.55.9.679.

Ilamparuthi, K., E. A. Dickin, and K. Muthukrisnaiah. 2002. "Experimental Investigation of the Uplift Behaviour of Circular Plate Anchors Embedded in Sand." *Canadian Geotechnical Journal* 39 (3): 648–664. https://doi.org/10.1139/t02-005.

Liu, J., M. Liu, and Z. Zhu. 2012. "Sand Deformation Around an Uplift Plate Anchor." *Journal of Geotechnical and Geoenvironmental Engineering* 138 (6): 728–737. Jun. https://doi.org/10.1061/(ASCE)GT.1943-5606.0000633.

Nagai, H., T. Tsuchiya, and M. Shimada. 2018. "Influence of Installation Method on Performance of Screwed Pile and Evaluation of Pulling Resistance." *Soils & Foundations* 58 (2): 355–369. Apr. https://doi.org/10.1016/j.sandf.2018.02.006.

Nagata, M., and H. Hirata. 2005. Study on Uplift Resistance of Screwed Steel Pile, *Nippon Steel Technical Report No. 92*. Tokyo, Japan: Nippon Steel & Sumitomo Metal Corporation, pp. 73–78.

Nazir, R., H. S. Chuan, H. Niroumand, and K. A. Kassim. 2014. "Performance of Single Vertical Helical Anchor Embedded in Dry Sand." *Measurement: Journal of the International Measurement Confederation* 49 (1): 42–51. https://doi.org/10.1016/j.measurement.2013.11.031.

Pérez, Z. A., J. A. Schiavon, Cristina de Hollanda Cavalcanti Tsuha, D. Dias, and L. Thorel. 2018. "Numerical and Experimental Study on Influence of Installation Effects on Behaviour of Helical Anchors in Very Dense Sand." *Canadian Geotechnical Journal* 55 (8): 1067–1080. Aug. https://doi.org/10.1139/cgj-2017-0137.

Perko, H. A. 2009. *Helical Piles: A Practical Guide to Design and Installation*. Hoboken, NJ, USA: John Wiley & Sons. https://doi.org/10.1002/9780470549063.

Sabermahani, M., and H. Nuri. 2021. "Studying the Effect of Geometrical Nail Layout on the Performance of Soil-Nailed Walls: Physical and Numerical Modeling." *Acta Geodynamica et Geomaterialia* 18 (1 (201)): 45–59. Feb. https://doi.org/10.13168/AGG.2021.0003.

Salehzadeh, H., H. Nuri, and A. A. H. Rafsanjani. 2022. "Failure Mechanism of Helical Anchors in Sand by Centrifuge Modeling and PIV." *The International Journal of Geomechanics* 22 (8): 1–20. https://doi.org/10.1061/(asce)gm.1943-5622.0002422.

Schiavon, J. A., C. de H. C. Tsuha, A. Neel, and L. Thorel. 2019. "Centrifuge Modelling of a Helical Anchor Under Different Cyclic Loading Conditions in Sand." *International Journal of Physical Modelling in Geotechnics* 19 (2): 72–88. Mar. https://doi.org/10.1680/jphmg.17.00054.

Schiavon, J. A., Cristina de Hollanda Cavalcanti Tsuha, and L. Thorel. 2016. "Scale Effect in Centrifuge Tests of Helical Anchors in Sand." *International Journal of Physical Modelling in Geotechnics* 16 (4): 185–196. https://doi.org/10.1680/jphmg.15.00047.

Schiavon, J. A., C. H. C. Tsuha, and L. Thorel. 2017. "Cyclic and Post-Cyclic Monotonic Response of a Single-Helix Anchor in Sand." *Géotechnique Letters* 7 (1): 11–17. Mar. https://doi.org/10.1680/jgele.16.00100.

Sharif, Y. U., et al. 2021. "Assessing Single-Helix Screw Pile Geometry on Offshore Installation and Axial Capacity." Proceedings of the Institution of Civil Engineers -

Geotechnical Engineering, vol. 7, 1–18. Oct. https://doi.org/10.1680/jgeen.21.00104.

Sharif, Y. U., M. J. Brown, B. Cerfontaine, C. Davidson, M. O. Ciantia, J. A. Knappett J. D. Ball, et al. 2021. "Effects of Screw Pile Installation on Installation Requirements and In-Service Performance Using the Discrete Element Method." *Canadian Geotechnical Journal* 58 (9): 1334–1350. Sep. https://doi.org/10.1139/cgj-2020-0241.

Spagnoli, G., and C. de Hollanda Cavalcanti Tsuha. 2020. "A Review on the Behavior of Helical Piles as a Potential Offshore Foundation System." *Marine Georesources & Geotechnology* 38 (9): 1013–1036. Feb. https://doi.org/10.1080/1064119X.2020.1729905.

Spagnoli, G., K. Gavin, C. Brangan, and S. Bauer. 2015. "In Situ and Laboratory Tests in Dense Sand Investigating the Helix-to-Shaft Ratio of Helical Piles as a Novel Offshore Foundation System." In *Frontiers in Offshore Geotechnics III*, no. MAY, edited by V. Meyer, 643–648. London: CRC Press. https://doi.org/10.1201/b18442-85.

Stanier, S. A., J. A. Black, and C. C. Hird. 2014. "Modelling Helical Screw Piles in Soft Clay and Design Implications." *Proceedings of the Institution of Civil Engineers - Geotechnical Engineering* 167 (5): 447–460. https://doi.org/10.1680/geng.13.00021.

Stanier, S. A., and D. J. White. 2013. "Improved Image-Based Deformation Measurement in the Centrifuge Environment." *Geotechnical Testing Journal* 36 (6): 915–928. https://doi.org/10.1520/GTJ20130044.

Tsuha, C. H. C., N. Aoki, G. Rault, L. Thorel, and J. Garnier. 2012. "Evaluation of the Efficiencies of Helical Anchor Plates in Sand by Centrifuge Model Tests." *Canadian Geotechnical Journal* 49 (9): 1102–1114. https://doi.org/10.1139/t2012-064.

Urabe, K., K. Tokimatsu, H. Suzuki, and Y. Asaka. 2015. "Bearing Capacity and Pull-Out Resistance of Wing Piles during Cyclic Vertical Loading." 6th International Conference on Earthquake Geotechnical Engineering, Christchurch , New Zealand, November.

White, D. J., W. A. Take, and M. D. Bolton. 2003. "Soil Deformation Measurement Using Particle Image Velocimetry (PIV) and Photogrammetry." *Géotechnique* 53 (7): 619–631. Sep. https://doi.org/10.1680/geot.2003.53.7.619.

Zhang, D. J. Y. 1999. *Predicting Capacity of Helical Screw Piles in Alberta Soils*. University of Alberta.